Preprints of the 19th World Congress
The International Federation of Automatic Control
Cape Town, South Africa. August 24-29, 2014

A Non-raster Scanning Approach in Atomic Force Microscopy Using a Combined Contour Prediction Algorithm

Kaiqiang Zhang* Guido Herrmann* Christopher Edwards Stuart C Burgess* Mervyn Miles*****

**Department of Mechanical Engineering, University of Bristol, UK (e-mail: kz12008@my.bristol.ac.uk; g.herrmann@bristol.ac.uk; s.c.burgess@bristol.ac.uk)*
*** Engineering Department, University of Exeter, UK (e-mail: C.Edwards@exeter.ac.uk)*
****School of Physics, University of Bristol, UK (e-mail: m.j.miles@bristol.ac.uk)*

Abstract: In this paper, we present a novel non-raster scanning algorithm for high-speed imaging in Atomic Force Microscopy. In contrast to recent non-raster scanning algorithms for string-like samples, the proposed algorithm is developed for cells and other simple specimen samples. This algorithm collects data in the vicinity of the specimen to create sample contours at different heights to build the 3D topography of the target sample. During the scan process, the tip is steered based on a prediction of the contour curvature and contour tangent. The proposed scanning trajectory follows the contour of the sample and avoids crossing the specimen, while minimizing the possible excitation of resonances of the cantilever. For the prediction of the curvature and tangent of the contour, the current partially obtained contour and a previous contour scan are used: a prediction from both contours is suitably combined by a weighting algorithm derived from a reliability evaluation of both predictions. This permits the creation of topographical images of specific interest at a reduced scanning time in comparison to some prevalent non-raster scan algorithms and raster scans. Simulation results are provided.

1. INTRODUCTION

In this paper, we describe and illustrate a novel non-raster scanning algorithm for imaging simple object samples, like cells, in Atomic Force Microscopy (AFM). Practically the interaction force between a very sharp cantilever-tip and the specimen-substrate is collected as the measurements in AFM (Binning et. al., 1986). The tip is commonly driven along a collection of parallel horizontal lines as the scanning raster. In this way, the 3D topographical image of the scanned substrate is constructed pixel-by-pixel along the raster. Thus, it often takes several seconds or even minutes to scan the entire substrate, depending on the quality, resolution, and size requirements of the imaging. Such a long scanning time restricts the applications of AFM (e.g. Picco et. al., 2007).

Researchers are actively striving to decrease the scanning time while ensuring the imaging quality in AFMs. Most of their research can be classified by: a) mechanical improvements (Schitter and Rost, 2008; Picco et. al., 2007), b) advanced vertical (z-axis) control (e.g. Wu et. al., 2009; Pao et. al., 2007), and c) design of optimal tip trajectories to achieve a complete scan image similar to but more efficiently than raster scans (Yong et. al., 2010; Tuma et. al., 2012). Thus, one significant similarity of all the above mentioned approaches is to achieve a scan pattern for a given fixed scan area while ignoring the information of the actual specimen and information collected from it. In contrast, a series of non-raster scanning algorithms (Andersson, 2007; Chang and Andersson, 2008; Chang et. al., 2011; Huang and Andersson, 2011, 2013) have been developed by Andersson for string-like samples, e.g. DNA, using the past measurements as a-priori knowledge. These non-raster scanning algorithms scan the vicinity of string-like samples by creating an estimated curve model from measured data (e.g. Huang and Andersson, 2013, for an experimental verification). Thus, the scanning time is reduced by just focusing on the wanted area as the whole specimen.

However, all these approaches have several limitations: For instance, raster scans create a high demand on the accuracy and bandwidth of the vertical cantilever height control (z-axis control), while collecting possibly specimen-irrelevant data (Abramovitch et. al., 2007). The tip-z-axis-control has to follow the sample surface in high-speed scans, e.g. scanning along a raster-scanning trajectory or along a designed spiral trajectory. Thus, the sharp high-speed tip has to go across the specimen surface and may damage the sample. In contrast, recent non-raster scanning approaches for string-like samples or boundary tracking can decrease the scanning time by reducing unwanted data collection. However, in biomedical research, it is necessary to scan the whole surface for cells or objects and not just scan the boundaries (Müller and Dufrêne, 2011).

Motivated by eliminating some of these limitations, we develop a non-raster scanning algorithm for simple object samples, which are smooth and have neither cross points nor links on their sample contours, similar to cells. The surface profile of such a sample can be treated as a collection of contours at different heights. We suggest scanning several contours of the target sample, where each contour can be used to predict the next contour in the specimen topography. For each contour scan, the tip can be steered in the vicinity of the contour at a fixed height above the substrate; thus, the fixed AFM tip height avoids issues usually connected with z-control in AFM. Extending ideas from non-raster scanning (Andersson, 2007; Chang and Andersson, 2008; Huang and

Andersson, 2013), the underlying methodology of the proposed scanning algorithm is to consider not only knowledge from the current partially obtained contour, but also from a previous contour scan, to construct a prediction of the current contour for more efficient data collection and to remain close to the specimen.

2. ANDERSSON'S NON-RASTER SCANNING METHOD AND A TRAJECTORY FOR OBJECT SAMPLES

In this paper, we only focus on simple object samples, like cells. For such a sample, the contour can be modelled as a solid, smooth boundary at one height. Therefore, we consider the basic idea and the curve estimation schemes of Andersson's non-raster scanning method (Andersson, 2007; Chang and Andersson, 2008; Huang and Andersson, 2013) as the starting point of our proposed algorithm.

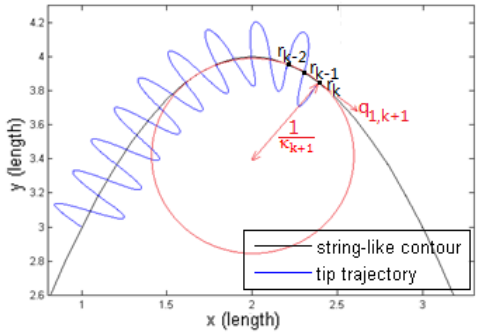

Fig. 1. An illustration of Andersson's non-raster scanning algorithm with smooth trajectory and contour prediction. The tangent vector $q_{1,k+1}$ and the curvature κ_{k+1} are estimated by (2) and (3) for the tip-control in real-time according to three new measured points r_k, r_{k-1}, and r_{k-2}.

At any fixed height, the contour for a string-like, continuous specimen (e.g. DNA) or for the continuous, smooth boundary of a specimen can be modelled as a curve in a plane. Thus, the spatial evolution of the contour can be given in the Frenet-Serret Frame by

$$r'(s) = dr(s)/ds = q_1(s) \quad (1.a)$$

$$q_1'(s) = dq_1(s)/ds = \kappa(s)q_2(s) \quad (1.b)$$

$$q_2'(s) = dq_2(s)/ds = -\kappa(s)\, q_1(s) \quad (1.c)$$

where r(s) stands for the position vector in the fixed frame with arclength s on the curve, $q_1(s)$ is the tangent vector at the point, $q_2(s)$ is the normal vector with respect to point r(s) and $\kappa(s)$ is the curvature at point r(s) . The arclength variable s is a function of time t. The function s(t) is defined for the scanning process through a desired scan velocity.

In recent non-raster scanning methods, the tip motion trajectory is determined by the data associated with the current contour scan. Practically, the tip is moved along smooth sine segments around the estimated curve (see Fig. 1). During one boundary scan, the estimation of the curvature and the tangent of the curve is updated with each triple of newly obtained points r_k, r_{k-1}, and r_{k-2} on the curve in real-time. Here r_k stands for the k-th measured point on the curve in the Cartesian coordinates frame. Assuming a very small arclength difference in s between each two adjacent points on the boundary, the curvature and tangent at point r_k is approximated from r_k, r_{k-1}, and r_{k-2}. Therefore, the k+1-th curve "states" can be estimated from the data at the k-th step. For the heading direction of the current tip motion, the tangent vector $q_{1,k+1}$ and normal vector $q_{2,k+1}$ approximately satisfies

$$q_{1,k+1} = \frac{r_{k-1}-r_k}{\|r_{k-1}-r_k\|},\ q_{2,k+1} = \begin{bmatrix} 0 & -1 \\ 1 & 0 \end{bmatrix} q_{1,k+1} \quad (2)$$

Here the Euclidean distances, $d(\cdot,\cdot)$, between each two points among r_{k-2}, r_{k-1}, and r_k are $a = d(r_{k-2}, r_{k-1})$, $b = d(r_{k-1}, r_k)$ and $c = d(r_{k-2}, r_k)$ (see Figure 1). Based on Heron's formula (e.g. Andersson, 2007), the curvature estimation for the k+1-th sample is given by

$$\kappa_{k+1} = \pm 4\sqrt{\frac{\ell(\ell-a)(\ell-b)(\ell-c)}{abc}},\ \ell = \frac{1}{2}(a+b+c) \quad (3)$$

where κ_{k+1} is the k+1-th curvature estimation. When the cosine of the angle between the vector (r_{k-1}, r_k) and the normal vector is positive, the κ_{k+1} takes positive sign. Otherwise, κ_{k+1} is negative.[1]

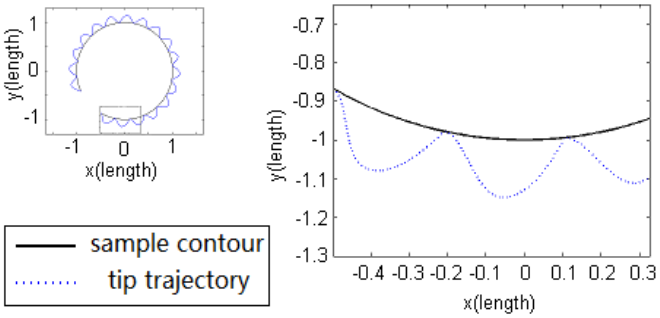

Fig. 2. Example of the proposed trajectory for scanning object samples. Here the curvature of the target contour is constant, while the amplitude is A = 0.2, and ω = 0.1.

Developed from Andersson's smooth trajectory (Chang and Andersson, 2008), a novel trajectory is introduced in Fig. 2, which is constructed in two parts: a) a sine-curve to send the tip towards the sample contour to allow measuring points on the contour; b) a cosine-curve to move away from the contour, thus, avoiding the crossing of the sample when a point on the contour is measured. For any instant s_1, s_2, …, where $r_d(s_i)$ describes a point on the contour, the tip trajectory is defined by

$$r_t(s-s_i) = \begin{cases} r_d(s-s_i) + \frac{A}{2}\left(1-\cos\left(2\omega(s-s_i)\right)\right)q_2(s-s_i), \\ \quad \text{for } 0 \le s-s_i \le \frac{\pi}{2\omega} \\ r_d(s-s_i) + A\sin\left(\omega(s-s_i)\right)q_2(s-s_i) \\ \quad \text{for } \frac{\pi}{2\omega} \le s-s_i \end{cases} \quad (4)$$

for $s\text{-}s_i \ge 0$. Here A denotes the amplitude of the scanning trajectory, ω is the spatial frequency of the trajectory, q_2 is the normal vector to the contour. r_d indicates the estimated contour position and r_t is the demanded cantilever tip position as a function of arclength s. Thus, the two parts of the

[1] Measurement noise might be amplified: Here a Kalman filter is recommended to reduce the noise influence (see Andersson, 2007).

trajectory are smooth and certainly continuously joined at the joining point $s - s_i = \frac{\pi}{2\omega}$. Moreover, the tangent of the scanning trajectory coincides with the contour tangent for $s \to s_i+$, which avoids crossing into the specimen and introduces the least possible change in tangent at $s = s_i$.

The performance of the proposed scanning trajectory is influenced by the amplitude A and the spatial frequency ω. This is similar to Chang and Andersson (2008, 2009), which point out, that A determines the search region of the trajectory, i.e. the trajectory is ensured to measure a point on the contour with large enough A. The scalar ω determines the frequency of collecting data. A large value for ω implies a high density of points along the contour in the current scan.

Practically, the tip is to be controlled with respect to time t. To derive a function s(t), we propose a constant tip velocity $v_{tip} = dr_{tip}/dt$ to ensure the trajectory is as smooth as possible, thus, avoiding the excitation of the dynamics in the cantilever-tip system and the actuators. Considering the time derivative of the tip position in the Frenet-Serret frame and the requirement for a constant tip velocity $\|v_{tip}\| = const.$, we compute from (4) and (1)

$$\|v_{tip}\| = \left\|\frac{dr_{tip}(t)}{dt}\right\| = f(s)\frac{ds}{dt} \tag{5}$$

where a function f(s) is defined by

$$f(s) = \begin{cases} \sqrt{\left(1 - \frac{A}{2}\kappa - \frac{A}{2}\kappa\cos(2\omega s)\right)^2 + (A\omega\sin(2\omega s))^2} \\ \text{for } 0 \le s(t) - s_i \le \frac{\pi}{2\omega} \\ \sqrt{(1 - A\kappa\sin(\omega s))^2 + (A\omega\cos(\omega s))^2} \\ \text{for } \frac{\pi}{2\omega} \le s - s_i \end{cases}$$

so that $\|v_{tip}\|dt = f(s)\,ds$. Under the assumption of a constant tip velocity, the relationship between s and t is calculated by an integral operation as $\|v_{tip}\|t = \int_0^s f(\rho)d\rho$. This permits the calculation of arclength s as a function of time t. For real time AFM imaging, the function s(t) has to be calculated offline a-priori. Specifically, the function t(s) can be approximated by curve-fitting. Then the inverse of the function t(s) is the function of s with respect to time t.

3. WEIGHTED PREDICTION ALGORITHM

3.1 A Recursive Least Square Prediction Method

When scanning simple object samples, nearby contours are similar to each other and it can be assumed that there is some projection (translation, scaling and rotation) which relates these close contours. Therefore, a currently partially scanned contour can be estimated using information from previously scanned contours. Here, we propose a least squares approximation of the currently scanned contour depending on previously scanned data.

In practice, the suggestion is to scan the target sample starting with contours at lower height, advancing to the top point of the specimen; this is sensible as the uncertainty at the very top contour is the most significant due to noise. The current scanning contour is always higher and in diameter/area smaller than previously scanned contours. Thus, the currently scanned contour may be called the inner contour, Y, and the previously scanned contour is the outer contour, X.

Suppose the measured points from the previous scan are $X = [X_1, X_2, \dots, X_k, ..]$, where each point $X_k = [X_{kx} \quad X_{ky}]^T$ is represented in Cartesian coordinates. Due to the small distances between the points in X, the centre (the mean) of X_k, $C = \left[\frac{\sum_k X_{kx}}{N} \quad \frac{\sum_k X_{ky}}{N}\right]^T$, can be used as a reference point for a map between a point on the outer contour X to a point on the inner contour Y; N denotes the number of obtained points in X. The normalized vector from one point X_k on the outer contour to the centre C is defined as $V_k = \frac{X_k - C}{\|X_k - C\|}$. To find a relationship between the inner and outer contours, suppose one point Y_k on the inner contour is obtained from the point X_k on the outer contour along the vector V_k. In this way, Y_k, can be mapped from X_k by transformation as

$$Y_k = \mathcal{A}X_k + \mathcal{B}\,, \text{ or } Y_k = [\mathcal{A}|\mathcal{B}]\begin{bmatrix} X_k \\ 1 \end{bmatrix} \tag{6}$$

where $\mathcal{A}$ is a two-by-two matrix and $\mathcal{B}$ is a vector with 2 elements. Here matrix $\mathcal{A}$ can represent a rotation or a contraction towards the centre point C, whiles B represents a simple translation. As a result, the currently scanned inner contour can be estimated from the previous outer contour and an appropriate transformation map.

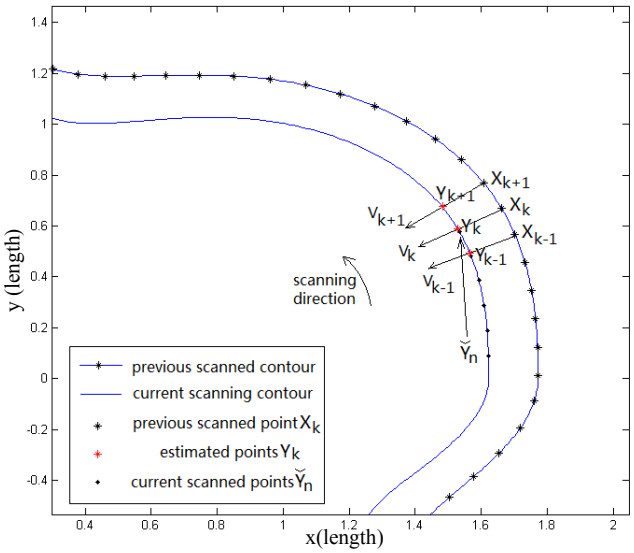

Fig. 3. Demonstration of a prediction using the RLS filter. The transformation map (6), and (9) from the outer contour and the inner contour is calculated by Y_k and X_k, which are obtained by finding the closest cross point of V_k and the partly measured inner contour close to the current point $\breve{Y}_n$.

However, an accurate approximation of the map $[\mathcal{A}|\mathcal{B}]$ is not available a priori. Thus, a recursive least squares (RLS) approach is proposed to estimate the map, which allows an incremental improvement of the map. Thus, it is necessary for the contour Y to obtain some initial measurement values $\breve{Y}_1, \breve{Y}_2, \dots$ within the current inner contour scan without the use of the map $[\mathcal{A}|\mathcal{B}]$. This creates a growing sequence of discrete points $\breve{Y}$ measured on the inner contour: $\breve{Y} = [\breve{Y}_1, \breve{Y}_2, \dots, \breve{Y}_n]$, where $\breve{Y}_i$ represent the measured points on the

(partially) measured inner contour and n is the number of obtained points on the currently scanned contour. In the current inner contour scan, Y_k is proposed as the closest crossing point of V_k on the contour line created by $\check{Y}$. The point X_k is the starting point of the vector V_k to provide Y_k.

Thus, when the tip measures a new point on the inner contour, the points $Y_k = [Y_{kx} \quad Y_{ky}]^T$ on the currently scanned contour and $X_k = [X_{kx} \quad X_{ky}]^T$ on the outer contour are obtained. The transfer map can be rewritten as

$$Y_{kx} = w_x{}^{\mathrm{T}} \begin{bmatrix} X_k \\ 1 \end{bmatrix}, Y_{ky} = w_y{}^{\mathrm{T}} \begin{bmatrix} X_k \\ 1 \end{bmatrix} \tag{7}$$

where w_x and w_y are two vectors defining the map $[\mathcal{A}|\mathcal{B}]$; $Y_{k,x}$ and $Y_{k,y}$ denote the x and y values of Y_k. Therefore the RLS updating equations at time k are given by

$$\mathrm{N_{k,m}} = \mathrm{H_{k,m}} \begin{bmatrix} X_k \\ 1 \end{bmatrix} \tag{8.a}$$

$$K_{k,m} = \frac{\mathrm{N_{k,m}}}{\lambda + \begin{bmatrix} X_k \\ 1 \end{bmatrix}^{\mathrm{T}} \mathrm{N_{k,m}}} \tag{8.b}$$

$$\theta_{k,m} = Y_{k,m} - w_{k,\mathrm{m}}{}^{\mathrm{T}} \begin{bmatrix} X_k \\ 1 \end{bmatrix} \tag{8.c}$$

$$w_{k+1,m} = w_{k,m} + K_{k,m}\theta_{k,m} \tag{8.d}$$

$$\mathrm{H_{k+1,m}} = \lambda^{-1}\mathrm{H_{k,m}} - \lambda^{-1}K_{k,m} \begin{bmatrix} X_k \\ 1 \end{bmatrix}^{\mathrm{T}} \mathrm{H_{k,m}} \tag{8.e}$$

Here $m = x$ or y indicates the index in terms of the relevant Cartesian coordinate elements. The scalar λ is a constant, positive parameter, which is set to be equal to or smaller than 1. Often it is set slightly less than 1. For initialization, all elements in w_k equal to 0 and H_k is an identity matrix. Thus, with the RLS filter, the map is estimated online for the current contour scan by

$$[\mathcal{A}|\mathcal{B}] = [w_x \quad w_y]^{\mathrm{T}}. \tag{9}$$

In the RLS filtering process, the most recently updated information influences the results more than old data (Haykin, 2001), depending on the choice of λ. Therefore, the estimated map will be adaptive to the changing inner contour. The next section will suggest a suitably weighted combination of this RLS-based algorithm with the contour prediction algorithm of Andersson from Section 2 (Chang and Andersson, 2008).

3.2. Combined prediction via adaptive weighting

Andersson's prediction algorithm in Section 2 provides a contour estimation from three new scanned points on the current contour (2)-(3). Here we name this prediction as the current-prediction, because such a prediction of curve states is only based on information from the currently scanned contour. The estimated heading direction and curvature are introduced as θ_{cur} and κ_{cur}. On the other hand, the RLS-prediction described in Section 3.1 predicts the next points based on both the currently scanned inner and the recently scanned outer contour. With these estimated points, the curve states as heading angle θ_{RLS} and κ_{RLS} can be calculated.

In this work, we propose a prediction algorithm, which combines the current-prediction and the RLS-prediction to achieve an increased accuracy. In practice, two estimated contour states, which are given by $[\theta_{cur} \quad \kappa_{cur}]^T$ and $[\theta_{RLS} \quad \kappa_{RLS}]^T$, are weighted to provide the prediction of the contour model for driving the tip. A simple weighting law is

$$\begin{bmatrix} \theta_e \\ \kappa_e \end{bmatrix} = \mathrm{W_{cur}} \begin{bmatrix} \theta_{cur} \\ \kappa_{cur} \end{bmatrix} + \mathrm{W_{RLS}} \begin{bmatrix} \theta_{RLS} \\ \kappa_{RLS} \end{bmatrix}, \mathrm{W_{RLS}} + \mathrm{W_{cur}} = 1 \tag{10}$$

The errors from the two predictions are introduced as the variables to be used for evaluating the weights. With the estimation method introduced by Andersson (2007), the estimated position of a point on the curve can be calculated from the update law using the curve states via

$$P_k = \bar{P}_{k-1} + \begin{cases} \frac{\mathrm{M}(\kappa_k \mathrm{ds})}{\kappa_k} \begin{pmatrix} q_{1k} \\ q_{2k} \end{pmatrix}, \kappa_k \neq 0 \\ q_{1k}\mathrm{ds}, \kappa_k = 0 \end{cases} \tag{11}$$

where $\mathrm{M}(\alpha) = \begin{pmatrix} \sin\alpha & 0 & 1-\cos\alpha & 0 \\ 0 & \sin\alpha & 0 & 1-\cos\alpha \end{pmatrix}$.

Here P_k represents the predicted point at arclength s where the (k-1)-th point $\bar{P}_{k-1}$ is measured. Here, κ_k, q_{1k}, and q_{2k} represent the estimates of the k-th curve states (see (2)-(3) in Section 2). Thus, the current-prediction and the RLS-prediction gives two estimates of the position of the point as $P_{cur,k}$ and $P_{RLS,k}$ at arclength s. With a new measured point $\bar{P}_k$ on the contour, the Euclidean distances from $\bar{P}_k$ to $P_{cur,k}$ and $P_{RLS,k}$ are introduced as the errors in the two prediction methods. Here the Euclidean distances are used as the evaluation variables for the following reasons: a) low computational complexity, b) ease of evaluation compared to the errors of estimated contour states, c) simplicity of use as a one dimensional value. Thus, the errors of the current-prediction and the RLS-prediction are defined by

$$\mathrm{e_{cur.k}} = \|P_{cur.k} - \bar{P}_k\|_2 \ , \ \mathrm{e_{RLS.k}} = \|P_{RLS.k} - \bar{P}_k\|_2 \tag{12}$$

where $e_{cur.k}$ and $e_{RLS.k}$ indicate the errors of current-prediction and RLS-prediction separately.

To avoid the effect of considerable noise in the errors, the weights from the two predictions are obtained by (statistically) averaging the errors of both predictions over time. Additionally, the current estimation performance is more important than old data for accurate contour tracking performance. Therefore an update algorithm, using a filter approach, was utilized to assess the errors of the two predictions:

$$\widehat{\mathrm{W}}_{\mathrm{cur.k}} = \mathrm{e_{cur.k}} + \alpha\widehat{\mathrm{W}}_{\mathrm{cur.k-1}} \tag{13.a}$$

$$\widehat{\mathrm{W}}_{\mathrm{RLS.k}} = \mathrm{e_{RLS.k}} + \alpha\widehat{\mathrm{W}}_{\mathrm{RLS.k-1}} \tag{13.b}$$

where $\widehat{W}_{cur}$ and $\widehat{W}_{RLS}$ are the filter variables for the current-data-prediction and the RLS-prediction and α is a forgetting parameter to consider the history of the errors. Then the weights W_{cur} and W_{RLS} are obtained by normalizing the updates $\widehat{W}_{cur}$ and $\widehat{W}_{RLS}$ as

$$\mathrm{W_{cur}} = \frac{\widehat{\mathrm{W}}_{\mathrm{RLS}}}{\widehat{\mathrm{W}}_{\mathrm{RLS}} + \widehat{\mathrm{W}}_{\mathrm{cur}}}, \mathrm{W_{RLS}} = \frac{\widehat{\mathrm{W}}_{\mathrm{cur}}}{\widehat{\mathrm{W}}_{\mathrm{RLS}} + \widehat{\mathrm{W}}_{\mathrm{cur}}}. \tag{14}$$

At the beginning of the scanning of one contour, W_{cur} is initialized as 0 and W_{RLS} is 1, while $\widehat{W}_{cur}$ and $\widehat{W}_{RLS}$ are set to 0 since there is no efficient estimation from the current-prediction methods until three points on the contour have been obtained. They will be calculated after the first three points on the contour have been measured. In addition, the

forgetting parameter α is a positive constant smaller than 1. When α equals 1, all historical errors can influence the weighted prediction.

As more points are measured, the overall performance of the weighted prediction improves, i.e. the curve is estimated with an increasing accuracy. There is no need for driving the tip with a very large searching region to ensure an efficient error-free scan. The tip can be kept in a very small neighbourhood to the sample contours. Therefore, the parameter A, which determines the tip searching range, can be adjusted to the prediction accuracy. One possible adaptive A is designed as

$$A = \begin{cases} A_{\max} & \text{if } \max\left[\widehat{W}_{\text{cur}}, \widehat{W}_{\text{RLS}}\right] \geq A_{\max} \\ A_{\min} & \text{if } \max\left[\widehat{W}_{\text{cur}}, \widehat{W}_{\text{RLS}}\right] \leq A_{\min} \\ \max\left[\widehat{w}_{\text{cur}}, \widehat{W}_{\text{RLS}}\right], & \text{elsewhere} \end{cases} \quad (15)$$

Here, parameter $A_{\min}$ is set as the smallest amplitude of the tip trajectory and parameter $A_{\max}$ is set as the maximal scanning amplitude. As a consequence, the tip can move away from or closer to the contour boundary for measuring the next point on the curve. In this way, the impact of considerable noise in the error can be eliminated to some extent.

In practice, at the beginning of the scanning process, the statistically weighted prediction is not available due to a lack of knowledge about the sample's shape. Thus, as suggested in Section 3.1, a scan from the bottom of the specimen is essential for initialization at first. The scan height should be set from the surface of the substrate to scan the first contour of the target specimen as an initial scan using the proposed novel trajectory together with Andersson's prediction algorithm (Chang and Andersson, 2008). Then, the proposed weighted scanning algorithm can be applied for contour scans at stepped different fixed (constantly increasing scanning) heights. An issue is that the tip will fail to scan the top of the sample, because the uppermost contour has a too small scale. Thus, the non-raster scanning algorithm should be terminated before the very top of the target sample is reached.

4. SIMULATION RESULTS

In order to evaluate and illustrate the proposed algorithm, the original data from a $(1.6\mu m)^2$ bacteria image were processed for the simulation experiment. The original bacteria image (Fig. 4. a) was obtained from a raster scan by Dazzi (2013). The left-upper bacterium (Fig. 4. a) was used as the target sample. In our approach, the sample topography is assumed to be smooth and continuous. Therefore, the original image was resized into $1nm^2$/pixel by the Bicubic interpolation method and smoothened by a Gaussian filter (Fig. 4. b).

The height scale in Fig. 4 and Fig. 5 is from 0 nm to 300 nm. However, the images are processed as 256 levels of colour in Matlab. Thus, the 300nm length on the z-axis is divided into 256 units, by which means each height unit stands for 1.18nm. This height "unit" of 1.18 nm will be used in the following simulations in Matlab. For the x-y coordinates, one horizontal unit is 1nm. In the simulation tests, we introduce Gaussian noise with 0 expectation and 1 unit standard deviation when "measuring" the above processed $1nm^2$/pixel data. The parameters of the proposed non-raster scan were set to ω = 0.2, $A = A_{max}$ = 30nm, A_{min} = 5nm, α = 0.6, and λ = 0.99 for successful contour scans. To achieve the scanning accuracies of ~$(5nm)^2$/pixel, ~$(10nm)^2$/pixel, and ~$(20nm)^2$/pixel, the scanning step size for the scan height were 5 units, 10 units, and 20 units. Clearly, in the x-y plane, the scanned contour defines the scanned image. Thus, a scan with a high, targeted pixel accuracy may not be completely dense, covering every single pixel of the targeted scan area. For the simulation, it is assumed that the linear scan speed with respect to time t is constant, i.e. ||dr/dt|| = const. = 500μm/s.

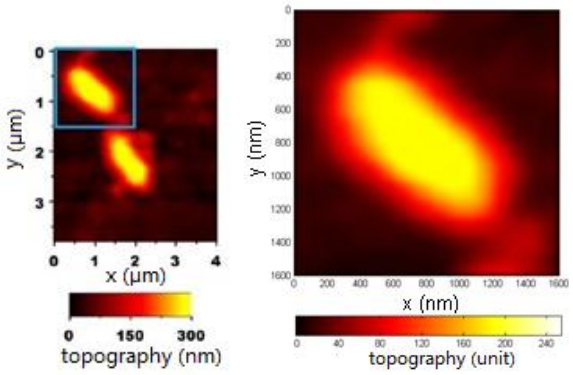

(a) (b)

Fig. 4. The original data (a) from AFM raster scan (Dazzi, 2013); the processed, smoothened data (b)

Simulations showed that the proposed non-raster scanning algorithm requires about only 60% of the time of the raster scanning algorithm (see Table 1). Fig. 5. b includes one illustration of a $(10nm)^2$/pixel imaging experiment. The white trace is the tip trajectory at 155unit height, recorded within a period of 0.016s. In contrast, we applied Andersson's approach (Chang and Andersson, 2008; Chang et. al., 2011) for a simulated contour scan (see Fig. 5. a). Using the same ω = 0.2, both approaches can successfully scan the sample contour with almost the same accuracy, i.e. both scanning algorithms scan the same number of points on the target contour (158 points in Fig. 5. a and 164 points in Fig. 5. b). However, Andersson's approach required 0.024s to produce the contour scan. Moreover, our proposed algorithm avoids damaging the specimen as it does not cross the higher part of the sample surface during the high-speed scan.

Using the proposed non-raster scanning algorithm, the image can be reconstructed from the original non-raster scanned data successfully in, e.g. reconstruction of $(10nm)^2$/pixel image as in Fig. 5. c. Note also the small 'empty' patches, which the scan contours have not covered. This is certainly only a problem if the gradients in the sample are high. Nevertheless, the non-raster scanning generically avoids 'jump' effects in raster scans which result from a low bandwidth in the height control, i.e. z-control.

Table 1. A comparison of raster and non-raster scanning time

Scanning resolution	Time for raster scanning	Time for non-raster scanning
$(20nm)^2$/pixel	0.256 s	0.172 s
$(10nm)^2$/pixel	0.512 s	0.299 s
$(5nm)^2$/pixel	1.024 s	0.614 s

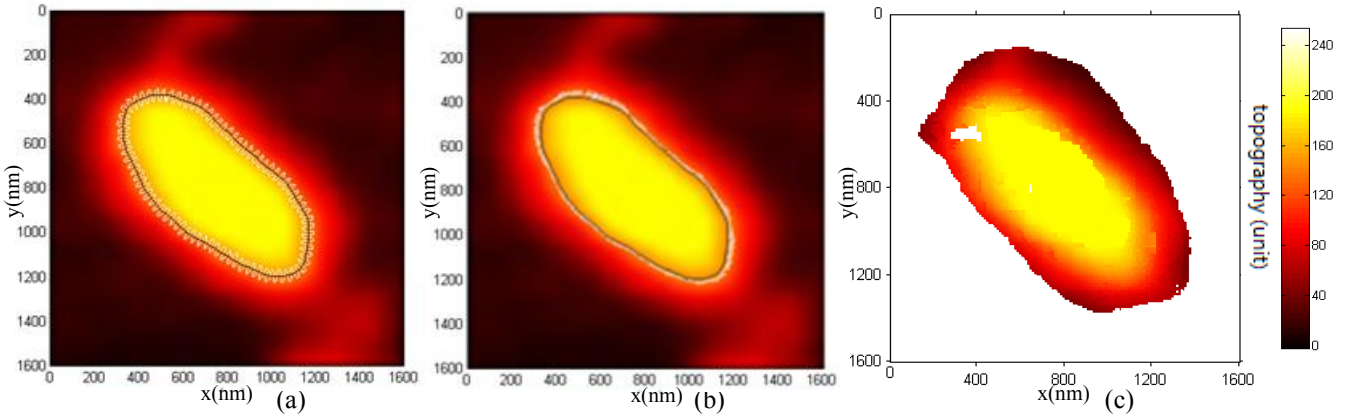

Fig. 5. Examples of contour scans at 155unit height with 10unit step-size using Andersson's approach (a) (Chang et. al., 2011) and the proposed method (b); reconstructed image (c) using the proposed non-raster scan (10unit step-size).

In the simulations, we found that the proposed imaging quality of the non-raster scanning algorithm is influenced by the detection frequency ω, and the height step size. The "blank" segments in the reconstructed data can be resolved by interpolation algorithms (e.g. Huang and Andersson, 2011) or by scanning with a larger ω. Moreover, the step size of the scanning height z determines the imaging quality. Here we only focus on the novel scanning algorithm; the influence of these parameters will be investigated in the future.

5. CONCLUSIONS

In this paper, we have proposed a novel non-raster scanning algorithm, which achieves high speed scanning for simple object samples compared with raster scans. A new scanning trajectory is introduced to avoid damage to the specimen, as the trajectory will not cross into the specimen. Moreover, the trajectory permits a dynamically adjusted amplitude, while a prediction algorithm fuses information from the currently scanned and the most recently scanned contour. Practically relevant simulations show that overall this provides faster non-raster scanning than recent contour scanning approaches and raster scanning approaches. Practical experiments on Bristol's probe microscopes are being planned.

REFERENCES

Abramovitch, D.Y., S. B. Andersson, L.Y. Pao. (2007). A tutorial on the mechanisms, dynamics, and control of atomic force microscopy. *American control conference 2007*, pp. 3488-3502. New York City, USA.

Andersson, S.B. (2007). Curve tracking for rapid imaging in AFM. *IEEE transactions on Nanobioscience*, **Vol. 6**, **No. 4**, pp. 354-361.

Binning, G., C.F. Quate, and C. Gerber. (1986). Atomic force microscope. *Physic Review Letters*, **Vol. 56**, pp. 930-933.

Chang, P.I., P. Huang, J. Maeng, and S.B. Andersson. (2011). Local raster scanning for high-speed imaging of biopolymers in atomic force microscopy. *Review of scientific instruments*, **Vol. 82**, 063603.

Chang, P.I., S.B. Andersson. (2008). Smooth trajectories for imaging string-like samples in AFM: a preliminary study. *2008 American control conference*, pp. 3207-3212. Seattle, Washington, USA.

Chang, P.I., and S.B. Andersson. (2009). Theoretical bounds on a non-raster scan method for tracking string-like samples. *2009 American control conference*, pp. 2266-2271. St. Louis, MO, USA.

Dazzi, A. (2013). AFM-IR: Infrared sub-cellular imaging with an atomic force microscope. [Online]. *Azonano.com*, *AZoM. Com Pty.Ltd*. [Available from: http://www.azonano.com/article.aspx?ArticleID=2921#2d]. [Accessed on 23th August].

Haykin, S.O. (2001). *Adaptive filter theory* (4th edition). Chapter 9. Prentice-Hall Inc, Upper Saddle River, New Jersey, USA.

Huang, P., and S.B. Andersson. (2011). Generating images from non-raster data in AFM. *2011 American control conference*, pp. 2246-2251. San Francisco, CA, USA.

Huang, P., and S.B. Andersson. (2013). Experimental verification of high speed AFM through local raster scanning. *2013 American control conference*, pp. 6063-6068. Washinton, DC, USA.

Müller, D.J. and Y.F. Dufrêne. (2011). Atomic force microscopy: a nanoscopic window on the cell surface. *Trends in cell biology*, **Vol. 21**, **issue 8**, pp. 461-469.

Pao, L.Y, J.A. Butterworth, and D.Y. Abramovitch. (2007). Combined feedforward/feedback control of atomic force microscopy. *Proceedings of the 2007 American control conference*, pp. 3509-3515. New York City, USA.

Picco, L.M., L. Bozec, A. Ulcinas, D.J. Engledew, M. Antognozzi, M.A. Horton, and M.J. Miles. (2007). Breaking the speed limit with atomic force microscopy. *Nanotechnology*, **Vol. 18**, 044030.

Schitter, G. and M.J. Rost. (2008). Scanning probe microscopy at video-rate. *Materialstoday*, **Vol. Microscopy special issue**, pp. 40-48.

Tuma, T., J. Lygeros, A. Sebastian, and A. Pantazi. (2012). Optimal scan trajectories for high-speed scanning probe microscopy. *2012 American control conference*, pp. 3781-2788. Fairmont Queen Elizabeth, Montréal, Canada

Wu, Y., Q. Zou, and C. Su. (2009). A current cycle feedback iterative learning control approach for AFM imaging. *IEEE transactions on Nanotechnology*, **Vol. 8**, **No. 4**, pp. 515-527.

Yong, Y.K., S.O.R. Moheimani, and I.R. Petersen. (2010). High-speed cycloid-scan atomic force microscopy. *Nanotechnology*. **Vol. 21**, 365503.